Ultrahigh ON/Off Current Ratio γ-Graphyne-1 Nanotube Based Sub 10 nm TFET Modeling and Simulation

Behrouz Rouzkhash (b.rouzkhash@email.kntu.ac.ir)
K N Toosi University of Technology Faculty of Electrical Engineering https://orcid.org/0000-0003-4158-1019

Alireza Salehi
K N Toosi University of Technology Faculty of Electrical Engineering

Mohammad Taghi Ahmadi
Urmia University of Technology

Research Article

Keywords: γ-graphyne-1, DFTB, TFET, I-V characteristic, mean free pass, subthreshold swing

Posted Date: January 3rd, 2022

DOI: https://doi.org/10.21203/rs.3.rs-1203103/v1

Abstract

Utilizing γ-graphyne-1 nanotubes (GyNTs) in the Tunneling Field Effect Transistors (TFETs) suppresses ambipolarity and enhances subthreshold swing (SS) of TFETs which is because of large energy band gap and high electron effective mass of GyNTs. In this research analysis of structural, electronic and thermoelectric properties of γ-graphyne-1 family under the deformation potential (DP) approach reveals that electron-phonon mean free path (MFP) of an Armchair GyNT (3AGyNT) and Zigzag GyNT (2ZGyNT) are 45 and 290 *nm*, respectively. Therefore, ballistic transport of sub 10 nm 3AGyNT-TFETs and 2ZGyNT-TFETs in different channel lengths are investigated utilizing Non-Equilibrium Green's Function (NEGF) formalism in the DFTB platform. Ultrahigh Current Ratio (OOCR) value of 1.6 x 10^{10} at V_{DD} = 0.2 *V* and very low point SS of 5 *mV/dec* are belonged to the 3AGyNT-TFET with channel length of 9.6 *nm*. 2ZGyNT-TFETs shows higher on-state current and SS as well as lower OOCR than those of 3AGyNT-TFETs. A linear relationship between channel length and logarithmic off-state current is reported that is consistent with WKB approximation. The obtained results along with the ultralow power consumption of the suggested GyNT-TFETs, make them as replacement of digital silicon MOSFETs in the next generation nanoelectronic devices.

1 Introduction

During the last years, numerous theoretical and experimental efforts have been carried out to enhance the efficiency of MOSFETs with sub 10 nm gate lengths [1-4]. Thermionic emission (TE), which is the basis of operation of conventional MOSFETs, is the main obstacle to scale down the threshold voltage (V_{th}) and power dissipation of transistors by imposing a lower limit on its subthreshold swing (SS) equal to $60mV/dec$ at room temperature [5]. On the other hand, quantum mechanical tunneling current through the potential barrier of the channel is comparable with the I_{off} within the sub 10 nm gate lengths. Thereby MOSFETs suffer from a lower limit of SS and both simultaneously TE and tunneling currents in the off state.

GAA MOSFETs have the ideal geometrical structure to efficiently control the channel current and short channel effects (SCEs) to achieve SS levels as near to $60mV/dec$ as possible. As per International Technology Roadmap for Semiconductors (ITRS) and International Roadmap for Devices and Systems (IRDS) documents, lower limit of gate length in the silicon nanowire based GAA MOSFETs is $10nm$ and reduction of technology node is only achieved via monolithic 3D (M3D) integration by stacking several layers of devices after 2024 [6-8]. New structures and technologies together with the innovative materials have been vastly investigated by electronic industries and researchers to scale down channel length and/or SS of MOSFETs. Nano-Electro-Mechanical gate FETs (NEMFETs) [9], ferroelectric dielectric FETs [10], negative capacitance FETs [11], and impact ionization FETs [12] have potentially lower SS than conventional MOSFETs. However the common drawback of these transistors is an intrinsic delay in their switching mechanisms [13].

TFETs are gated p-i-n junction devices which are biased in the reverse direction with ultralow SS and high mobility at room temperature. CNT based GAA TFETs (CNT-TFETs) are the appreciated homojunction transistors using semiconducting CNTs with $n \neq 3\nu$ in the source, channel, and drain region [14,15]. From a material point of view since sheet of graphene has metallic property, CNTs have this ability to convert channel of CNT-TFETs from semiconductor to metal by changing its chiral vector to $n = 3\nu$ which can degrade absolutely operation of a digital transistor. Hence CNTs has not enough reliability to use in the electronics industries which have a tendency of using always semiconducting channels in nanoelectronic devices particularly in high OOCR digital transistors [16].

Graphyne is another 2D allotrope of carbon that was predicted firstly by Baughman in 1987 [17]. Four types of high symmetry nanostructures of graphyne family are α, β, γ, and 6,6,12-graphynes. Among carbon allotropes consisting of all types of graphynes only γ-graphyne-n are intrinsic 2D semiconductors which have n acetylenic linkages consisting of two sp hybridized carbon atoms between hexagonal rings of sp^2 hybridized carbon atoms of graphene.

Using cross-coupling reaction, γ-graphyne-2 (graphdiyne) multilayer sheets and graphdiyne multiwall nanotube arrays were successfully fabricated by Guoxing Li *et al*. in 2010 and 2011, respectively [18,19]. It was shown that the graphdiyne sheets have semiconducting behavior. Qiaodan Li and teammates succeeded to synthesize monocrystalline single layer γ-graphyne-1 sheet through a mechanochemical reaction in 2018 [20]. The atomic and electronic structure of synthesized samples were characterized by XRD, XPS, EDX, TEM, and UV-visible spectrum. They found that the band gap energy and lattice constant of γ-graphyne-1 sheets are $2.53eV$ and $0.69nm$, respectively.

The previously calculated band gap energy of γ-graphyne-1 sheet in different DFT, HSE06, DFTB, and B3LYP methods shows diverse values of $0.45eV$ [21,22,16], $0.98eV$ [21,23], $1.28eV$ [21,24], and $2.23eV$ [25], respectively. The single aforementioned experimental result shows an overestimated band gap value of $2.53eV$ because of the presence of oxygen in the synthesized γ-graphyne-1 sheet.[20] The calculated band gap in DFT methods are usually underestimated, particularly in large band gap materials suchlike γ-graphyne-1 [26,25]. In this research, the calculated band gap energy in DFTB method is 1.34 eV agreed with the previous calculations and is between the comparably precise HSE06 method and the single experimental results [27,28]. Hence DFTB is a reliable method and is utilized in all calculations in this paper. The electronic and structural properties of γ-graphyne-1 sheets and nanotubes have been investigated and it is shown that the lower limit band gap energy of high diameter GyNTs is the band gap of γ-graphyne-1 sheet [27]. In 2016, Desai successfully synthesized a homojunction MOSFET with $3.9nm$ effective channel length. In this transistor gate was a metallic CNT with $1nm$ diameter and source-channel-drain material was a two layer MoS_2 that was electrostatically doped to n^+ in the source and drain regions via a bottom gate at $5V$ bias [4].

In this paper two GAA homojunction p-i-n TFETs are constructed in Virtual NanoLab (VNL) and investigated via ATK package using 2ZGyNT and 3AGyNT. For the first time relaxation time, mobility, and MFP of γ-graphyne-1 family are calculated. It was shown that electron MFP of 2ZGyNT and 3AGyNT is

359 and $52nm$, respectively. Ballistic transport calculations shows I_{on} of 2ZGyNT-TFETs is nearly 10^3 times of 3AGyNT-TFETs. Ultrahigh OOCR value of $8.9\text{x}10^{15}$ at $V_{th} - V_{gs} = 0.5V$ and ultralow point SS value of $5mV/dec$ at $V_{gs} = V_{th}$ are achieved, where V_{th} is threshold voltage. At the bias conditions of $V_{th} - V_{gs} = V_{ds} = 0.2V$ the calculated I-V characteristic of 3AGyNT-TFET with a channel length of $9.6nm$ shows OOCR and SS values of $1\text{x}10^4$and $19mV/dec$, respectively. The average SS and OOCR of 3AGyNT-TFET with $L_{ch} = 3.6nm$ are $59mV/dec$ and $2.4\text{x}10^3$, respectively. Impact of channel length on the performance of TFETs are considered via I-V characteristic of GyNT-TFETs in the subthreshold region which is compatible to WKB approximation.

2 Computational Methods

γ-graphyne-1 nanotubes and transistors are constructed in the *VNL* software. Atomistic calculations of GyNTs and GyNT-TFETs are carried out via ATK package. In the geometrical relaxation of GyNTs the atomic force tolerance is set to 0.01 *eV/*Å. The convergence criterion of hamiltonian energy is 10^{-5} in DFTB and DFT based calculations. Basis set of mio is used in the DFTB method. In the DFT method the core-valance interactions are calculated by PseudoDojo pseudopotential that is a norm-conserving Troullier–Martins pseudopotential. The basis set is set to the medium. The electron-electron interactions are taken into account by the exchange-correlation functional of the Perdew-Burke-Ernzerhof (PBE) approach of Generalized Gradient Approximation (GGA) [29]. The vacume space is more than 17 Å in the simulations. Monkhorst-Pack grid of k-points are used in the reciprocal lattice sampling in the k-space and is set to $1x1x70$ for 1D GyNTs. The real space grid is based on the mesh cut-off energy of $50Ry$. Bulk nanomaterials and devices are investigated at room temperature $300K$ in all simulations. Currents of the TFETs are calculated utilizing Landauer-Büttiker formula in the NEGF approach [30]:

$$I\left(V_b\right) = G_0 \int_{-\infty}^{+\infty} dE/e\left[f_L\left(E-\mu_L\right) - f_R\left(E-\mu_R\right)\right] T(E,V_{ds}) \quad (1)$$

where $G_0 = 2e^2/h = 77.4\mu S$ is the conductance of one level channel, e is the electron charge, $T(E,V_{ds})$ is the transmission coefficient in the V_{ds}, f_L and f_R are the Fermi-Dirac distribution functions, and μ_L and μ_R are the electrochemical potentials of the left and right electrodes, respectively.

3 Results And Discussion

The unit cell of γ-graphyne-1 contains of a basis of 12 carbon atoms. As depicted in Fig. 1a, 2D γ-graphyne-1 sheet has a chiral vector of $\mathbf{C_h} = \mathbf{na}_1 - \mathbf{ma}_2$, where $\mathbf{a}_1 = \mathbf{a}_0\mathbf{x}$ and $\mathbf{a}_2 = \mathbf{a}_0(-1/2\mathbf{x} + \sqrt{3}/2\mathbf{y})$ are lattice vectors and $\mathbf{x}$. $\mathbf{y}$ are unit vectors. The chiral vector in the zigzag and armchair directions are (*n*. *n*) and (*n*.0), respectively. Zigzag and armchair γ-graphyne-1 nanotubes are formed via rolling γ-graphyne-1 sheet alongside its zigzag and armchair chiral vectors, respectively. 2ZGyNT unit ring (UR) is constructed by rolling up a supercell consisting of 2 unit cells in the zigzag direction (2,2) and UR of 3AGyNT is constructed via (3,0) chiral vector, as shown in Figs. 1b and c.

As acetylenic linkages in the sheet of γ-graphyne-1 break up bonding between hexagonal rings of graphene, a gap grows up in the band structure of γ-graphyne family and turning them to the intrinsic semiconductors. Therefore, GyNT-TFETs are trustworthy devices and encouraged as a replacement for silicon nanowire GAA MOSFETs, while CNT-TFETs are not reliable devices.

To scale down size of TFETs, GyNTs with low diameter and high chemical stability are utilized. The 2AGyNT and 2ZGyNT are the smallest nanotubes but 2AGyNT has relatively lower chemical stability due to its low cohesive energy $E_{coh} = -8.13eV$ whereas 3AGyNT and 2ZGyNT with nearly equal $E_{coh} = -8.30eV$ have chemically higher stability. Besides diameter of 2AGyNT is $4.4nm$ with high in plain strain that causes to shrinkage length of its UR up to 2% [27]. As a result, in this paper two GAA homojunction p-i-n TFETs are constructed and investigated using 2ZGyNT and 3AGyNT with diameter values of 7.6 Å and 7.6√3/2= 6.6 Å, respectively.

The GyNT has heavily p^+ and n^+ doping in the source and drain regions, respectively. The only difference between n-i-n conventional MOSFETs and p-i-n TFETs is the doping of their sources from n+ to p^+. Thereby TE in the source is not able to excite enough electrons from valence band to conduction band, specifically in high energy band gap nanomaterials such as GyNTs. Therefore, the only remind current of TFETs is due to the transient of electrons via band to band tunneling (BTBT) in the on-state and direct tunneling in the off-state. The concentration of dopants in the source and drain regions are set to as high as values to align the Fermi level energies to their VBM and CBM, respectively.

The GyNTs are defect and dislocation free and channel regions of TFETs are intrinsic without ionized impurity atoms and unavoidable cross sections, so scattering of electrons in the channel is elastic at low temperatures. At room temperature transport of electrons are ballistic provided that their MFP are greater than the channel length. Electron-Longitudinal Acoustic (LA) phonon MFP (λ_e) of GyNT is much more than its LA phonon-phonon MFP [31] with value of $\lambda_{ph} = 15nm$ [32]. λ_e of γ-graphyne-1 sheet and GyNTs is calculated via $\lambda_e = v_{gr}\tau_{rlx}$ formula where v_{gr} and τ_{rlx} are group velocity and relaxation time of carriers, respectively. τ_{rlx} for electrons and holes is calculated via deformation potential (DP) theory. The dispersion relation expression utilizing parabolic approximation of band structure at LUMO and HOMO of graphyne is $E(k) = \hbar^2 k^2 / 2m^*$, where $\hbar$ is reduced plank's constant and m^* is effective mass of carriers that achieved by $m^* = \hbar^2 / \partial^2(E) / \partial k^2$. By taking into account electron-LA phonon scattering, Bardeen and Shockley in 1958 proposed an analytical formula under the effective mass approximation in the framework of DP theory to calculate relaxation time τ_{rlx} and mobility μ of carriers in 2D nanomaterials (Eq. (2)) [33-35]. Equation (3) is the amended formula for 1D nanomaterials [36,37]:

$$\tau_{rlx} = \frac{2\hbar^3 C}{3k_B T m^* DP^2} (2)$$

$$\tau_{rlx} = \frac{\hbar^2 C}{(2\pi k_B T)^{1/2} m^{*1/2} DP^2} (3)$$

where T is temperature, C is elastic constant, and DP is deformation potential constant. By investigation structural and electronic properties of γ-graphyne-1 sheet, 2ZGyNT, and 3AGyNT under the uniform strain in the range of -2% < $\Delta a/a_0$ < 2%, $C = 2\Delta E_{tot}/(S(\Delta a/a_0)^2)$) for 2D and $C = a_0 \partial^2 E/\partial a^2$ for 1D nanomaterials and $DP = \Delta E_{edge}/(\Delta a/a_0)$ are calculated and m^* is achieved using ATK package [36]. ΔE_{tot} is the average increasing in the total energy of γ-graphyne-1 sheet and nanotubes and ΔE_{edge} is shift of energy at the edge of CBM and VBM for electrons and holes, respectively.

As depicted in Table 1, the relaxation time τ_{rlx} and mobility $\mu = e\tau_{rlx}/m^*$ of γ-graphyne-1 sheet for holes are $0.52ps$ and $3.18\text{x } 10^3 cm^2 V^{-1} s^{-1}$, respectively, agree with the previous calculations and for electrons are $1.05ps$ and $7.39\text{x } 10^3 cm^2 V^{-1} s^{-1}$, respectively, lower than those of previous calculations which is due to the lower calculated value of m^* in the DFT method relative to the DFTB method [38,35].

The relaxation time and mobility of 2ZGyNT are nearly one order of magnitude higher than those of 3AGyNT, as illustrated in Table 1. It is because of both simultaneously higher m^* and DP of 3AGyNT in contrast with 2ZGyNT. Higher DP constant reveals higher electron-phonon coupling of 3AGyNT relative to 2ZGyNT. MFP of electrons and holes of 2ZGyNT and 3AGyNT are greater than the maximum channel length of $10nm$ in this paper that cannot impose severely transmission of carriers through the channel. As a result, scattering of carriers in sub 10 nm 2ZGyNT-TFETs and 3AGyNT-TFETs are elastic and the transistors work in ballistic regime.

Two TFETs are constructed in VNL utilizing URs of 2ZGyNT and 3AGyNT. Each UR of 2ZGyNT and 3AGyNT has 48 and 72 carbon atoms with length values of 6.893 6 Å and 12.061 6 Å and diameters of 7.6 6 Å and 6.6 6 Å, respectively. Fig. 2 shows 2ZGyNT-TFET with gate length value of $5.5nm$ comprising of 8URs. 2ZGyNT-TFETs and 3AGyNT-TFETs have 4 and 3 URs with doping concentration of $0.003$and $0.008e/atom$, respectively, in the source and drain regions. Upper channel length of both zigzag and armchair sub 10 nm TFETs is $9.65nm$ with 14 and 8 URs under the gate, respectively.

Based on the WKB approximation transmission coefficient of a square potential barrier is:

$$T = \exp\left(-2L\sqrt{2m^* E_{bar}}/\hbar\right) (4)$$

where L and E_{bar} are length and height of potential barrier, m^* is effective mass of material, and $\hbar$ is reduced Plank's constant. Hence to maintain performance of TFETs in off-state it is essential to avoid from OOCR pinning via leakage current of insulator utilizing an oxide layer with enough high effective mass band gap product ($m^*_{ins}E_g^{ins}$) (Eq. (4)) with simultaneously high dielectric constant (K). SiO_2 is an excellent insulator with $m^*_{ins}E_g^{ins} = 0.42 \text{ x } 8.9 = 3.7$ but with a low K value of 3.9 [39]. $\mathrm{HfO2}$ with better $\mathrm{K} = 25$ has weak insulator property with $m^*_{ins}E_g^{ins} = 0.17 \text{ x } 5.7 = 0.97$ [40]. TiO_2 in Brookite phase has higher $m^*_{ins}E_g^{ins} = 1.46\text{x}3.5 = 5.1$ than $\mathrm{SiO2}$ and higher $\mathrm{K} = 80$ than $\mathrm{HfO2}$ and so has relatively

lower leakage current and higher performance than the other insulators [41]. Hence it is used as gate insulator material in this paper and previous investigation of TFETs [42].

I-V characteristic of 2ZGyNT-TFET with 8 URs in its channel (Fig. 2) on the bias conditions of $V_{ds} = 0.2V$ and $-2Vcript>$, is extracted and depicted in Fig. 3. Same curve of TFET is reproduced for Si and InAs nanowire TFETs utilizing WKB approximation [43]. It is obvious that a couple of unipolar transistors consisting of n-TFET and p-TFET are constructed with threshold voltages at $V_{th}^{n} = -0.3V$ and $V_{th}^{p} = -1.8V$, respectively. Contrary to the higher OOCR and lower SS of p-TFET relative to n-TFET, because of lower work function of metal gate in the n-TFET than p-TFET as well as higher mobility and MFP of electrons than those of holes, it is focused on the n-TFETs in this paper.

As shown in Fig. 3, I-V characteristic of TFET has 2 regions. At $V_{th}^{n}cript>$ and $V_{gs}cript>$ the TFET is in the saturation region. At $V_{th}^{n}cript>$ electrons can tunnel via BTBT from valence band of source, through a triangular potential barrier, to conduction band of channel and at $V_{gs}cript>$ holes can tunnel from conduction band of drain to valence band of channel. Between two BTBTs, gate voltage is in the range of $V_{th}^{p}cript>$ and TFET is in the subthreshold region in which I_{ds} is characterized by I_{on} and transmission coefficient of the channel.

Unlike conventional MOSFETs whose SS has a lower limit of $60mV/dec$, in the TFETs SS is not constant and has not lower limit, but instead is an increasing function of $m^{*}\left|V_{gs} - V_{th}\right|$ with the lowest value at $V_{gs} = V_{th}$ (Fig. 3).

By increasing negative voltage on the metal gate in the subthreshold region, $Log\left(I_{ds}\right)$ decreases on a nearly parabola curve versus V_{gs}, and SS gradually increases so the best point as on-state in a digital TFET is just near the V_{th} with the lowest value of SS. However in a digital TFET the average SS is desired not point SS that is slope of tangent line of I-V curve. The OOCR and average SS values of TFET in Fig. 3 are $6.8\mathrm{x}10^{3}$ and $52mV/dec$ for n-TFET, and$1.8\mathrm{x}10^{5}$ and $38mV/dec$ for p-TFET, respectively. Because of higher effective mass, p-TFET has higher OOCR and lower SS than n-TFET.

TFETs are ambipolar devices with total current of sum of the electron and hole currents in each V_{gs}. In the subthreshold region electron current is due to the direct tunneling of electrons from VB of source to CB of drain and hole current is due to the direct tunneling of holes in the opposite direction in the transmission window of eV_{ds}. Hence by increasing negative voltage of V_{gs} the electron current decreases while the hole current increases so ambipolarity causes the I-V characteristic of TFETs gradually deviate from curve of pure electron or hole current and finally at $V_{gsmin} = -1.1V$ two curves of electron and hole currents contact with each other with equal values and opposite slopes so slope of the I-V curve is zero and current value is two times of individual electron or hole currents. However the profile of potential barrier in the source-channel-drain is not constant and gradually changes with V_{gs} as

it helps to increase the current and finally at V_{gsmin} it increases more than 2 times of pure carrier curves. As a result to prevent from degradation of operation of a digital TFET by ambipolarity it is essential to select a nanomaterial with enough high energy band gap as $E_g/2 \gg eV_{DD}$.

By constructing 2ZGyNT-TFETs in different channel lengths $L_{ch} = nL_{UR}$ with n in the range of $7 \leq n \leq 14$, the impact of L_{ch} in the range of $4.8nmcript > .6nm$ on the performance of TFETs are investigated. The I-V characteristic of TFETs are calculated and depicted in Fig. 4. For n-TFETs and p-TFETs the $V_{th}^{n} \cong -0.3\mathrm{V}$ and $V_{th}^{p} \cong -1.8\mathrm{V}$, respectively.

Under the bias condition of $V_{th} - V_{gs} = 200mV$ and $V_{ds} = 200mV$, the OOCR and SS of TFETs are calculated and demonstrated in Fig. 5. It is obvious that $\mathrm{Log(OOCR)}$ is linear with respect to $L_{ch} = nL_{UR} = n\mathrm{x}0.69nm$. SS of n-TFET with 7 URs in the channel is $60.9mV/dec$, nearly equal to the minimum SS of MOSFETs. n-TFETs with channel length of 8 and 7 URs need $V_{th} - V_{gs} = 208mV$ and $V_{th} - V_{gs} = 244mV$ to get OOCR value of $1\mathrm{x}10^4$ nearly equal to the minimum requirement of OOCR as per ITRS [6].

It can be seen in Fig. 4, at every constant $V_{gs} = cte$ by increasing number of URs the current of TFETs decreases with nearly equal steps. As shown in Fig. 6, atomistic calculation shows a linear relationship between L_{ch} and $Log\left(I_{ds}\right)$ at $V_{gs} = cte$. Model of this relationship is $I_{off} \propto e^{-\alpha L_{ch}}$ that is consistent with the transmission coefficient of a square potential barrier based on the WKB approximation (Eq. (4)) and so the calculated approximation formula of I_{off} in the subthreshold region of the n-TFET is $I_{off} \approx I_{on}\exp(-6.5L_{ch}\sqrt{m^*(V_{th} - V_{gs})})$ [44,43]. For a precise model it is needed to take into account imaginary band dispersion of GyNTs in the WKB formula [43].

By increasing work function of metal gate by $eV_{off} = 0.5eV$ the I-V characteristic of TFETs shifts to the right so that the origin of the coordinates corresponds to the off-state and a plain curve of TFETs as digital transistors created. The TFETs are able to switch from off-state to on-state via $V_{gs} = 0.2V$.

γ-graphyne-1 armchair nanotubes have higher effective mass and lower mobility than zigzag nanotubes. So 3AGyNT-TFETs have potentially lower I_{on} and power consumption as well as higher OOCR than 2ZGyNT-TFETs. Fig. 7 shows a 3AGyNT-TFET with gate length value of $6nm$ which comprises of 5 URs.

On the bias condition of $V_{ds} = 0.2V$ and $-2.8Vcript >$, I-V characteristics of sub 10nm 3AGyNT-TFETs with $L_{ch} = nL_{UR}$ when n is in the range of $3 \leq n \leq 8$ are calculated and depicted in Fig. 8 and thereby the impact of channel length $3.6nmcript > .6nm$ on the performance of TFETs are investigated. As shown in Fig. 8, threshold voltage of n-TFETs and p-TFETs are $V_{th}^{n} \cong -0.5\mathrm{V}$ and $V_{th}^{p} \cong -2.5\mathrm{V}$, respectively. Red and blue shaded regions are two parts of subthreshold region of 3AGyNT-TFETs in which two digital n-TFETs and p-TFETs are constructed.

As shown in Fig. 9, $\mathrm{Log}(\mathrm{OOCR})$ and SS are linear and reciprocal functions of n, respectively. The minimum SS and maximum OOCR are belonged to the longest TFET with 8 URs in its channel where its OOCR at $V_{gs} = V_{gsmin} = -1.1V$ is $5.7\mathrm{x}10^{19}$ and its point and average SS at $V_{gs} = V_{th}^{n} = -0.5V$ and $V_{th}^{n} - V_{gs} = 0.2V$ are $5mV/dec$ and $19mV/dec$, respectively. n-TFET with $L_{ch} = 3L_{UR} = 3.6nm$ has \text{S}\text{S} value of 59 mV/dec. At {{V}_{th}^{n}-V}_{gs}=0.24 V its \text{O}\text{O}\text{C}\text{R} value reaches to {10}^{4}.

By increasing work function of metal gate by 0.7 eV the I-V characteristic of TFETs shifts to the right so that the n-TFETs are able to switch between off-state and on-state via {V}_{gs}=0.2 V.

4 Conclusion

Band gap engineering in γ-graphyne-1 hints its possible application in nanoelectronic device technology specially in FET platform. GyNT-TFETs due to their novel structure, material and technology with potential application as a high performance digital transistor in nanoelectronic devices requires deep investigation in physical point of view. In this study, the calculated electron MFP of GyNTs in the effective mass approximation and DP theory are enough high to perform reliable ballistic transport properties of sub 10 nm GyNT-TFETs. I-V characteristic of armchair and zigzag TFETs in different channel lengths are obtained. At channel length of 9.6 nm the 2ZGyNT-TFET and 3AGyNT-TFET show ultrahigh average \text{O}\text{O}\text{C}\text{R} value of 2x{10}^{7} and 1.2x{10}^{10}, respectively. 3AGyNT-TFET with channel length of 3.6 nmhas \text{S}\text{S} value of 59 mV/dec which is nearly equal to the minimum \text{S}\text{S} of conventional MOSFETs. A model of {I}_{off} based on the WKB approximation and linear relationship betweenLog\left({I}_{off}\right) and {L}_{ch} is proposed. At shorter channel lengths, future studies will be performed on optimizing the doping concentration and electrical field in the source and drain regions.

Declarations

Acknowledgment

The Makmal Nano in University Teknologi Malaysia for ATK software access is appreciated.

References

1. Ni, Z., Ye, M., Ma, J., Wang, Y., Quhe, R., Zheng, J., Dai, L., Yu, D., Shi, J., Yang, J., Watanabe, S., Lu, J.: Performance Upper Limit of sub-10 nm Monolayer MoS2 Transistors. Adv. Electron. Mater., 1600191-1600198 (2016). https://doi.org/10.1002/aelm.201600191

2. Zhou, W., Zhang, S., Guo, S., Wang, Y., Lu, J., Ming, X., Li, Z., Qu, H., Zeng, H.: Designing sub-10-nm Metal-Oxide-Semiconductor Field-Effect Transistors via Ballistic Transport and Disparate Effective Mass:

The Case of Two-Dimensional BiN. Phys. Rev. Appl. **13**, 1-9 (2020). https://doi.org/10.1103/PhysRevApplied.13.044066

3. Yang, J., Quhe, R., Li, Q., Liu, S., Xu, L., Pan, Y., Zhang, H., Zhang, X., Li, J., Yan, J., Shi, B., Pang, H., Xu, L., Zhang, Z., Lu, J., Yang, J.: Sub 10 nm Bilayer Bi2O2Se Transistors. Adv. Electron. Mater. **5**, 1-10 (2019). https://doi.org/10.1002/aelm.201800720

4. Desai, S.B., Madhvapathy, S.R., Sachid, A.B., Llinas, J.P., Wang, Q., Ahn, G.H., Pitner, G., Kim, M.J., Bokor, J., Hu, C., Wong, H.-S.P., Javey, A.: MoS2 transistors with 1-nanometer gate lengths. Science **354**(6308), 99-102 (2016). https://doi.org/10.1126/science.aah4698

5. Ionescu, A.M., Riel, H.: Tunnel field-effect transistors as energy-efficient electronic switches. Nature **479**, 329-337 (2011). https://doi.org/10.1038/nature10679

6. International Technology Roadmap for Semiconductors (ITRS). www.itrs2.net (2015).

7. International Roadmap for Devices and Systems (IRDS). https://irds.ieee.org/reports (2016).

8. International Roadmap for Devices and Systems (IRDS). https://irds.ieee.org/reports (2020).

9. Kim, J.-H., Chen, Z.C.Y., Kwon, S., Xiang, J.: Three-Terminal Nanoelectromechanical Field Effect Transistor with Abrupt Subthreshold Slope. Nano Lett. **14**(3), 1687–1691 (2014). https://doi.org/10.1021/nl5006355

10. CRISTOLOVEANU, S., WAN, J., ZASLAVSKY, A.: A Review of Sharp-Switching Devices for Ultra-Low Power Applications. IEEE J. Electron Devices Soc. **4**(5), 215-226 (2016). https://doi.org/10.1109/JEDS.2016.2545978

11. Tian, H., Li, Y.-X., Li, L., Wang, X., Liang, R., Yang, Y., Ren, T.-L.: Negative Capacitance Black Phosphorus Transistors With Low SS. IEEE Trans. Electron Devices **66**(3), 1579 - 1583 (2019). https://doi.org/10.1109/TED.2018.2890576

12. Musalgaonkar, G., Sahay, S., Saxena, R.S., Kumar, M.J.: An Impact Ionization MOSFET With Reduced Breakdown Voltage Based on Back-Gate Misalignment. IEEE Trans. Electron Devices **66**(2), 868 - 875 (2018). https://doi.org/10.1109/TED.2018.2887168

13. Seabaugh, A.C., Zhang, Q.: Low-Voltage Tunnel Transistors for Beyond CMOS Logic. Proc. IEEE **98**(11), 2095 - 2110 (2010). https://doi.org/10.1109/JPROC.2010.2070470

14. Tamersit, K.: Sub-10 nm junctionless carbon nanotube field-effect transistors with improved performance. Int J Electron Commun **124**, 10 (2020). https://doi.org/10.1016/j.aeue.2020.153354

15. Shirazi, S.G., Karimi, G.R., Mirzakuchaki, S.: GAA CNT TFETs Structural Engineering: A Higher ON Current, Lower Ambipolarity. IEEE Trans. Electron Devices **66**(6), 2822 (2019).

https://doi.org/10.1109/TED.2019.2912950

16. Wu, S., Yuan, Y., Cho, D., Lee, J.Y., Kang, B.: Chiral γ-graphyne nanotubes with almost equivalent bandgaps. J. Chem. Phys. **150**, 1-6 (2019). https://doi.org/10.1063/1.5065558

17. Baughman, R.H., Eckhardt, H., Kertesz, M.: Structure-property predictions for new planar forms of carbon: layered phases containing sp2 and sp atoms. J. Chem. Phys. **87**, 6687–6699 (1987). https://doi.org/10.1063/1.453405

18. Li, G., Li, Y., Qian, X., Liu, H., Lin, H., Chen, N., Li, Y.: Construction of Tubular Molecule Aggregations of Graphdiyne for Highly Efficient Field Emission. J. Phys. Chem. C **115**, 2611–2615 (2011). https://doi.org/10.1021/jp107996f

19. Li, G., Li, Y., Liu, H., Guo, Y., Lia, Y., Zhu, D.: Architecture of graphdiyne nanoscale films. Chem. Commun. **46**, 3256–3258 (2010). https://doi.org/10.1039/b922733d

20. Li, Q., Li, Y., Chen, Y., Wu, L., Yang, C., Cui, X.: Synthesis of γ-graphyne by mechanochemistry and its electronic structure. Carbon **136**(248-254) (2018). https://doi.org/10.1016/j.carbon.2018.04.081

21. Wu, W., Guo, W., Zeng, X.C.: Intrinsic electronic and transport properties of graphyne sheets and nanoribbons. Nanoscale **5**, 9264–9276 (2013). https://doi.org/10.1039/c3nr03167e

22. Hou, X., Xie, Z., Li, C., Li, G., Chen, Z.: Study of Electronic Structure, Thermal Conductivity, Elastic and Optical Properties of α, β, γ-Graphyne. materials **11**(2), 1-14 (2018). https://doi.org/10.3390/ma11020188

23. Kang, J., Li, J., Wu, F., Li, S.S., Xia, J.B.: Elastic, Electronic, and Optical Properties of Two-Dimensional Graphyne Sheet. J. Phys. Chem. C **115**, 20466–20470 (2011). https://doi.org/10.1021/jp206751m

24. Wang, X.-M., Lu, S.-s.: Thermoelectric Transport in Graphyne Nanotubes. J. Phys. Chem. C **117**(38), 19740-19745 (2013). https://doi.org/10.1021/jp406536e

25. Srinivasu, K., Ghosh, S.K.: Graphyne and Graphdiyne: Promising Materials for Nanoelectronics and Energy Storage Applications. J. Phys. Chem. C **116**, 5951–5956 (2012). https://doi.org/10.1021/jp212181h

26. Puigdollers, A.R., Alonso, G., Gamallo, P.: First-principles study of structural, elastic and electronic properties of α-β- and γ-graphyne. Carbon **96**, 879-887 (2016). https://doi.org/10.1016/j.carbon.2015.10.043

27. Rouzkhash, B., Salehi, A., Ahmadi, M.T.: Bandgap modulation of low-dimensional γ-graphyne-1 under uniform strain. J. Comput. Electron. **19**, 947–956 (2020). https://doi.org/10.1007/s10825-020-01521-6

28. Rouzkhash, B., Salehi, A., Ahmadi, M.T.: γ-Graphyne-1 band structure modeling and simulation. Solid State Commun. **325**, 114164 (2020). https://doi.org/10.1016/j.ssc.2020.114164

29. Perdew, J.P., Burke, K., Ernzerhof, M.: Generalized Gradient Approximation Made Simple. Phys. Rev. Lett. **77**(18), 3865-3868 (1996). https://doi.org/10.1103/PhysRevLett.77.3865

30. Buttiker, M., Imry, Y., Landauer, R., Pinhas, S.: Generalized many-channel conductance formula with application to small rings. Phys. Rev. B **31, no. 10**, 6207–6215 (1985). https://doi.org/10.1103/physrevb.31.6207

31. Reihani, A., Soleimani, A., Kargar, S., Sundararaghavan, V., Ramazani, A.: Graphyne Nanotubes: Materials with Ultralow Phonon Mean Free Path and Strong Optical Phonon Scattering for Thermoelectric Applications. J. Phys. Chem. C **122**(39), 22688–22698 (2018). https://doi.org/10.1021/acs.jpcc.8b05898

32. Ramazani, A., Reihani2, A., Soleimani, A., Larson, R., Sundararaghavan, V.: Molecular Dynamics Study of Phonon Transport in Graphyne Nanotubes. Carbon **123**, 635-644 (2017). https://doi.org/10.1016/j.carbon.2017.07.093

33. Bardeen, J., Shockly, W.: Deformation Potentials and Mobilities in Non-Polar Crystals. Phys. Rev. **80**(1), 72-81 (1950). https://doi.org/10.1103/PhysRev.80.72

34. PRICE, P.J.: Two-dimensional electron transport in semiconductor layers. I. Phonon scattering. Ann. Phys. **133**(2), 217-239 (1981). https://doi.org/10.1016/0003-4916(81)90250-5

35. Tan, X., Shao, H., Hu, T., Liu, G., Jiang, J., Jiang, H.: High thermoelectric performance in two-dimensional graphyne sheets predicted by first-principles calculations. Phys. Chem. Chem. Phys. **17**(35), 22872-22881 (2015). https://doi.org/10.1039/C5CP03466C

36. Long, M., Tang, L., Wang, D., Li, Y., Shuai, Z.: Electronic Structure and Carrier Mobility in Graphdiyne Sheet and Nanoribbons. ACS Nano **5**, 2593–2600 (2011). https://doi.org/10.1021/nn102472s

37. Beleznay, F.B., Bogar, F., Ladik, J.: Charge carrier mobility in quasi-one-dimensional systems: Application to a guanine stack. J. Chem. Phys. **119**(11), 5690-5695 (2003). https://doi.org/10.1063/1.1595634

38. Xi, J., Wang, D., Yi, Y., Shuai, Z.: Electron-phonon couplings and carrier mobility in graphynes sheet calculated using the Wannier-interpolation approach. J. Chem. Phys. **141**, 1-11 (2014). https://doi.org/10.1063/1.4887538

39. Chanana, R.K.: Determination of hole effective mass in SiO2 and SiC conduction band offset using Fowler–Nordheim tunneling characteristics across metal-oxidesemiconductor structures after applying oxide field corrections. J. Appl. Phys. **109**, 1-6 (2011). https://doi.org/10.1063/1.3587185

40. Liu, Q.-J., Liu, Z.-T., Feng, L.-P.: Electronic structure, effective masses and optical properties of monoclinic HfO2 from first-principles calculations. Adv. Mater. Res. **216**, 341-344 (2011). https://doi.org/10.4028/www.scientific.net/AMR.216.341

41. Landmann, M., Rauls, E., Schmidt, W.G.: The electronic structure and optical response of rutile, anatase and brookite TiO2. J. Phys.: Condens. Matter **24**, 1-6 (2012). https://doi.org/10.1088/0953-8984/24/19/195503

42. Ajay, Narang, R., Saxena, M., Gupta, M.: Two-dimensional (2D) analytical investigation of an n-type junctionless gate-all-around tunnel field-effect transistor (JL GAA TFET). J Comput Electron **17**, 713–723 (2018). https://doi.org/10.1007/s10825-018-1151-7

43. Luisiera, M., Klimeck, G.: Simulation of nanowire tunneling transistors: From the Wentzel–Kramers–Brillouin approximation to full-band phonon-assisted tunneling. J. Appl. Phys. **107**, 1-6 (2010). https://doi.org/10.1063/1.3386521

44. Sze, S.M., Ng, K.K.: Physics Of Semiconductor Devices, 3rd ed. Wiley, New Jersey (2006). https://doi.org/10.1002/0470068329

Tables

Table 1 Calculated electron and hole relaxation times, mobilities, and MFPs of *γ-graphyne-1* sheet, 2ZgyNT and 3AGyNT.

	***γ-graphyne-1* sheet**		**2ZGyNT**		**3AGyNT**	
	Electron	**Hole**	**Electron**	**Hole**	**Electron**	**Hole**
m^*/m_0	**0.25**	**0.29**	**0.23**	**0.28**	**0.43**	**0.52**
C [Jm^{-2}]	**762**					
C [$10^{10}eVcm^{-1}$]			**5.44**		**1.68**	
DP [eV]	**4.9**	**6.45**	**1.44**	**2.56**	**1.85**	**3.35**
τ_{rlx} [ps]	**1.05**	**0.52**	**2.49**	**0.71**	**0.34**	**0.10**
μ [$10^3cm^2V^{-1}s^{-1}$]	**7.39**	**3.18**	**19.04**	**4.48**	**1.40**	**0.37**
MFP [nm]	**160**	**57**	**359**	**77**	**52**	**11**

Figures

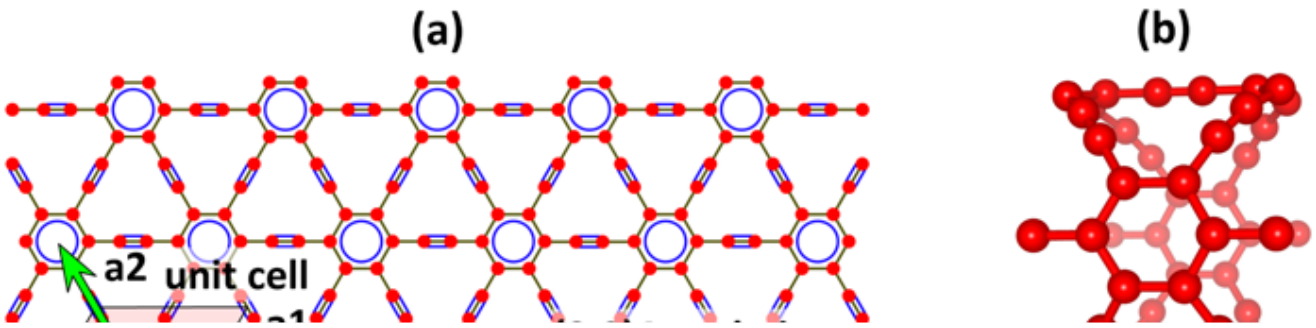

Figure 1

a) Unit cell as well as armchair and zigzag chiral vectors of *γ-graphyne-1 sheet*, b) unit ring of 2ZGyNT, and c) unit ring of 3AgyNT.

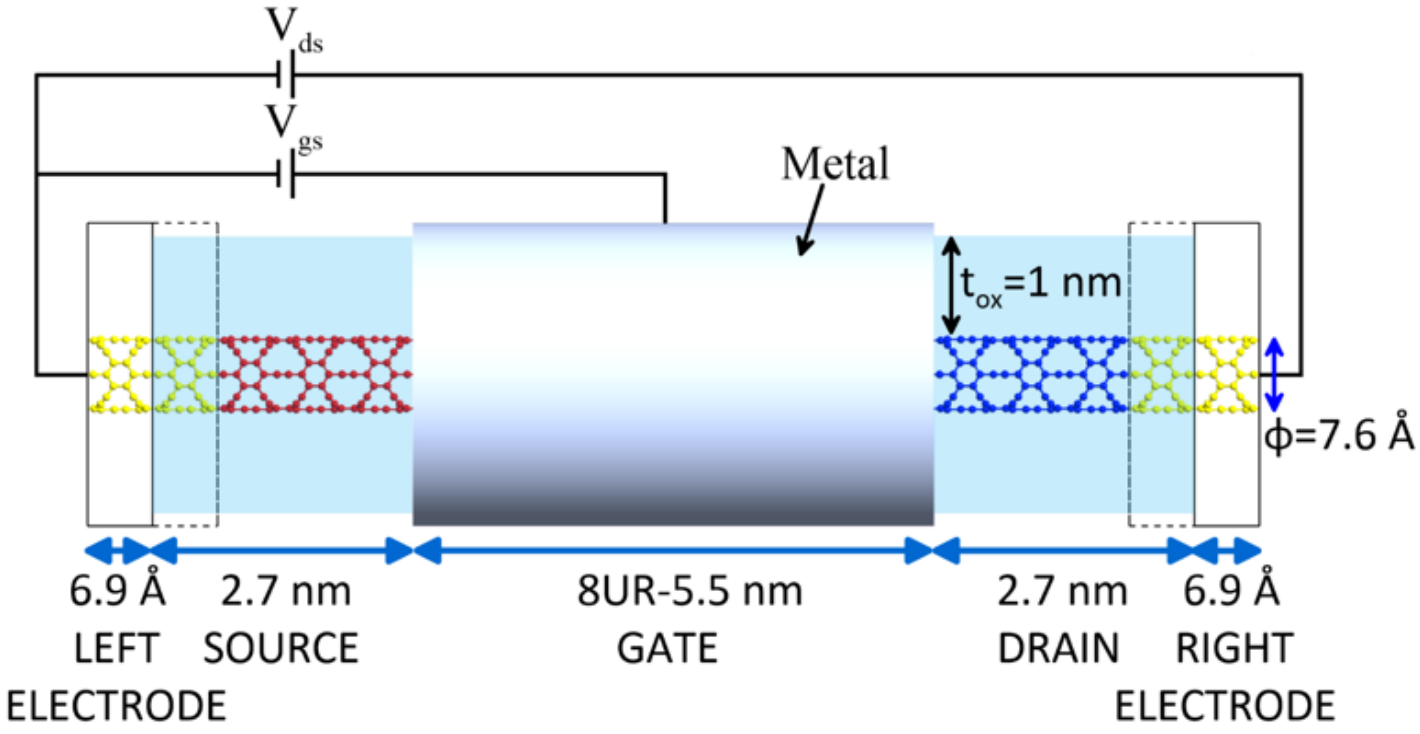

Figure 2

Schematic diagram of 2ZGyNT-TFET. Source and drain have p^+ (red) and n^+ (blue) doping, respectively. Doping concentration of source, drain, electrodes and extended electrodes is 0.003 *e/atom*.

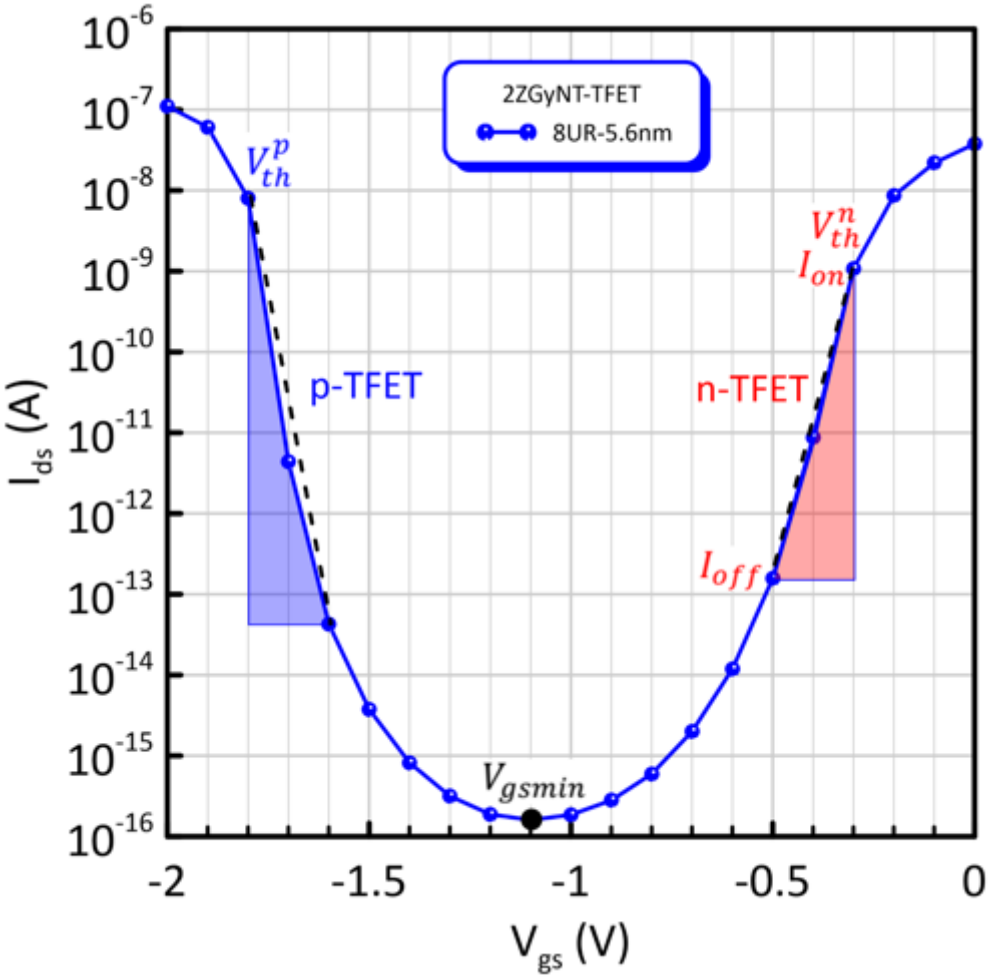

Figure 3

I-V characteristic of 2ZGyNT-TFET with 8 URs in its channel. Average SS of n-TFET and p-TFET, logarithmic slope of black dash lines versus vertical axis, are 49 and 37 *mV/dec*, respectively.

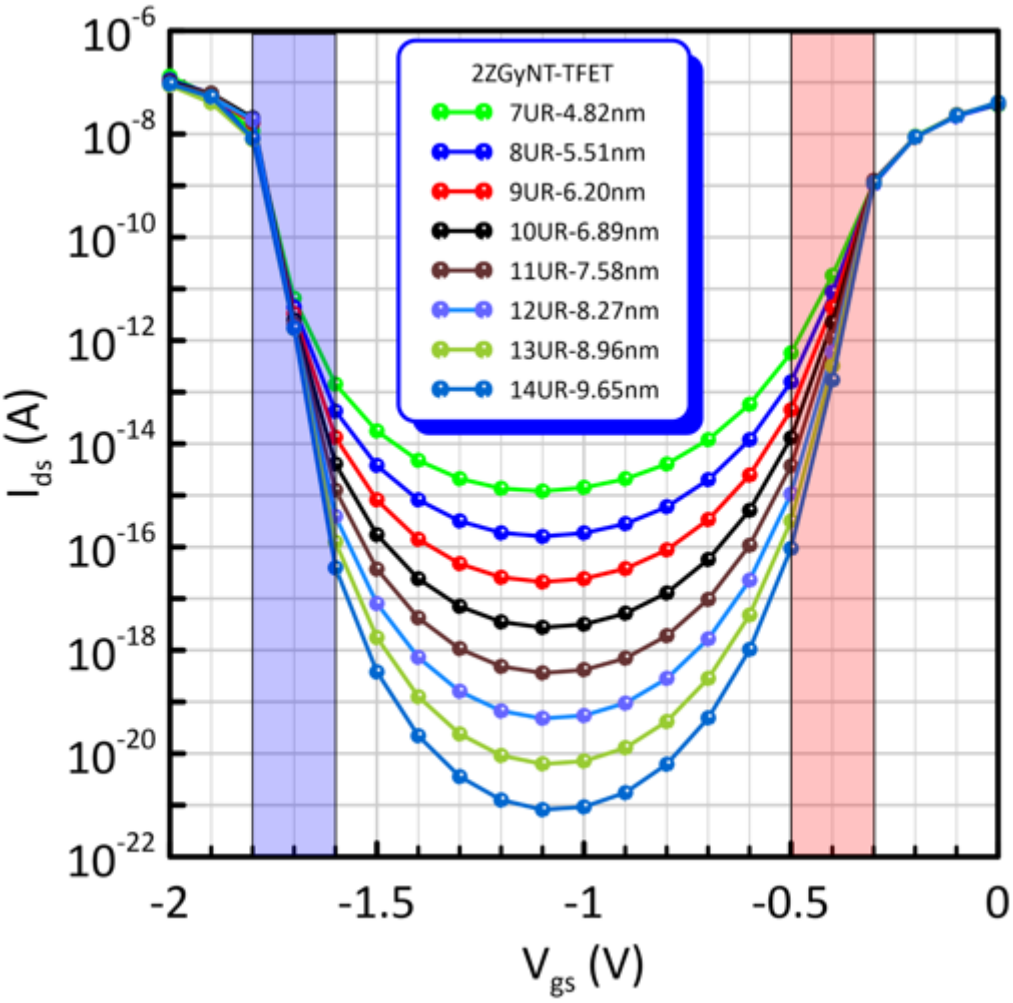

Figure 4

I-V characteristic of 2ZGyNT-TFETs. Red and Blue shaded areas are operational regions of n-TFETs and p-TFETs, respectively.

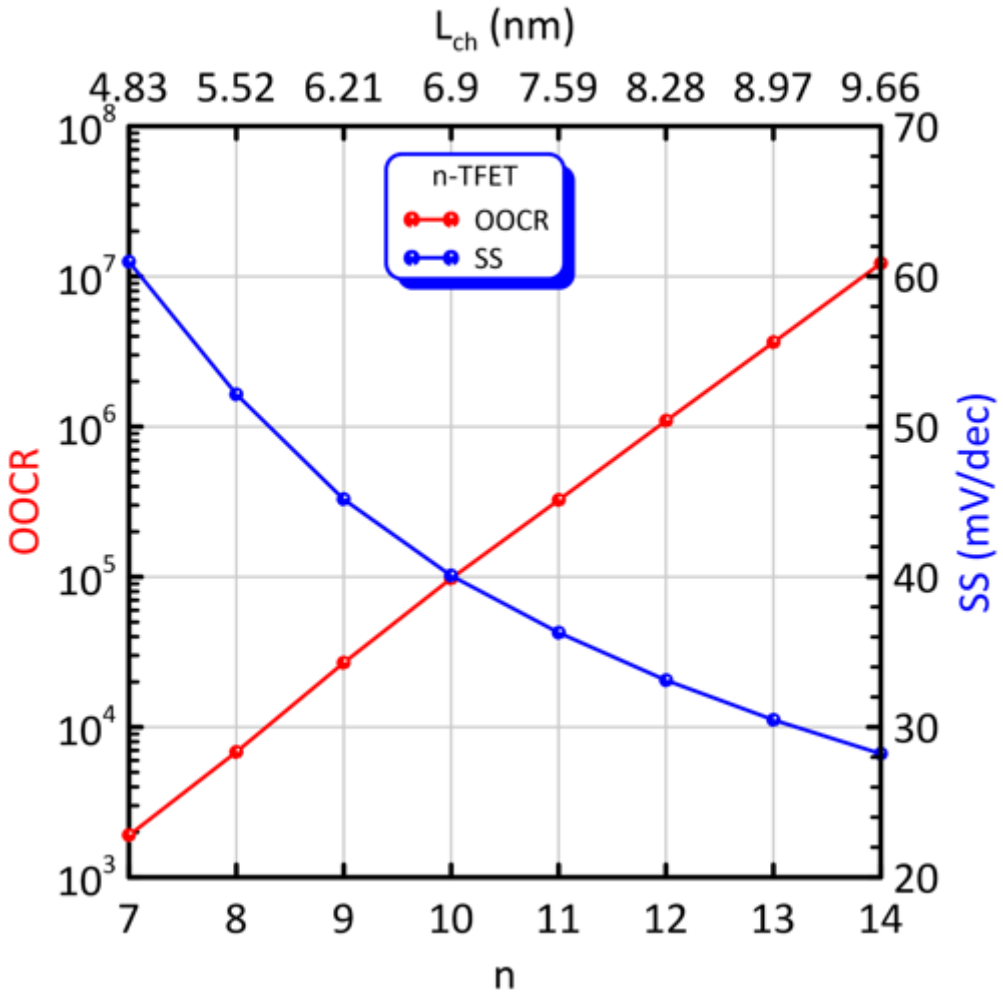

Figure 5

OOCR and of 2ZGyNT-TFETs. Log(OOCR) and SS are linear and reciprocal functions of L_{ch}, respectively.

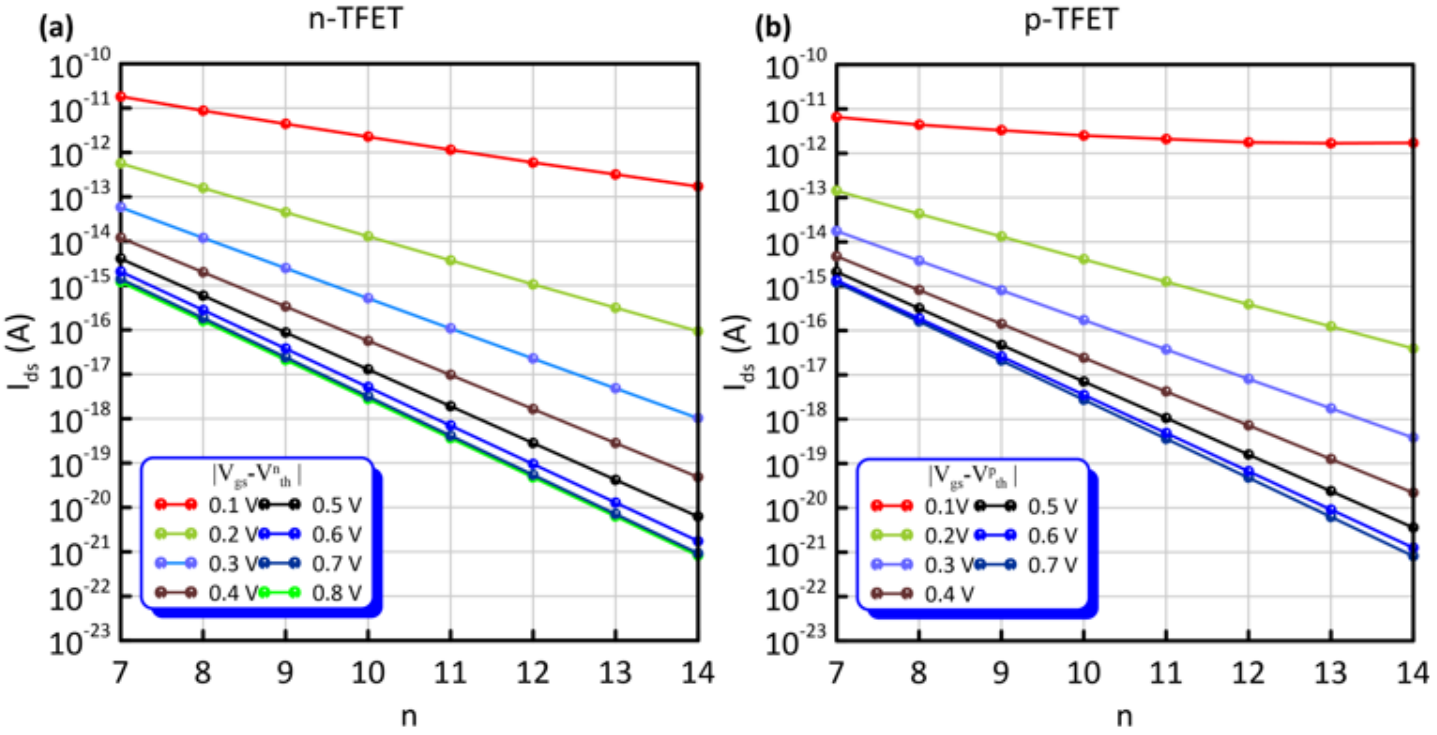

Figure 6

I-V characteristic of 2ZGyNT-TFETs at constant V_{gs} in the range of 0.1 $V < |V_{gs} - V_{th}| < |V_{gsmin} - V_{th}|$ for a) n-TFETs and b) p-TFETs.

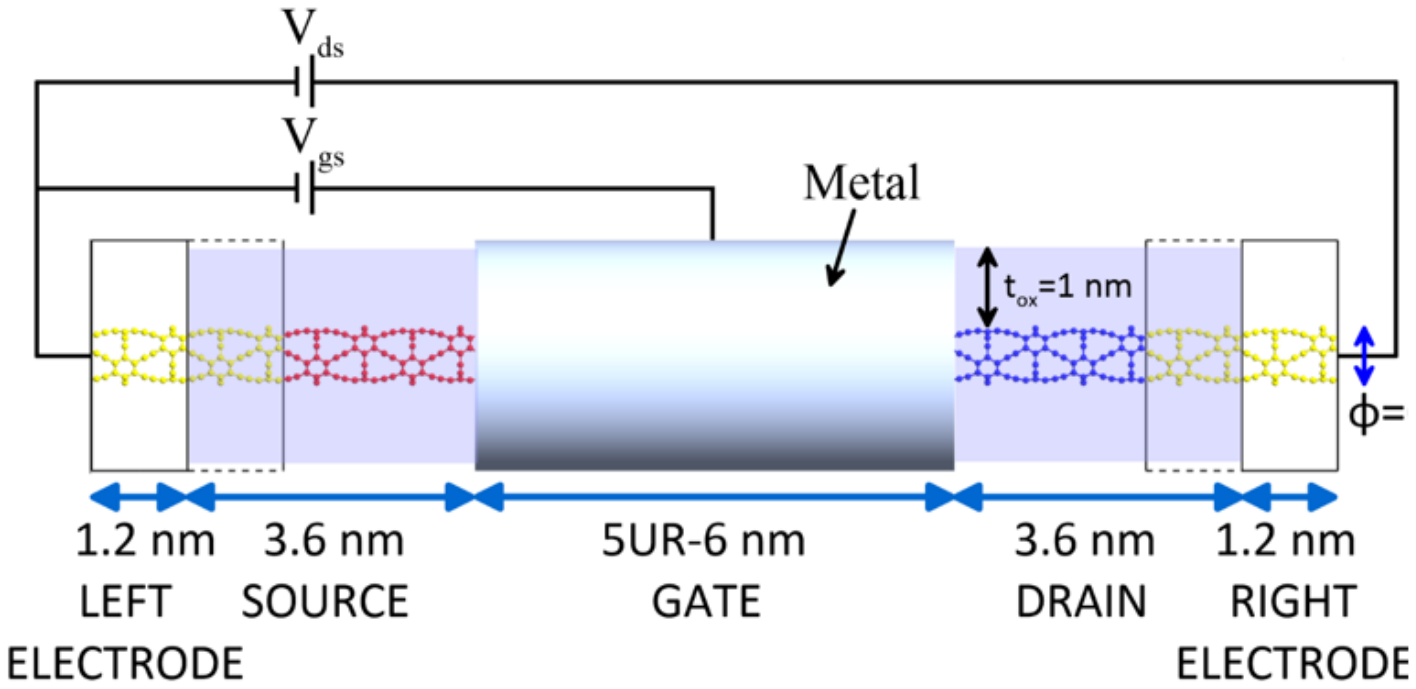

Figure 7

Schematic diagram of 3AGyNT-TFET. Source and drain have p^+(red) and n^+(blue) doping, respectively. Doping concentration of source, drain, electrodes and extended electrodes is 0.008 *e/atom*.

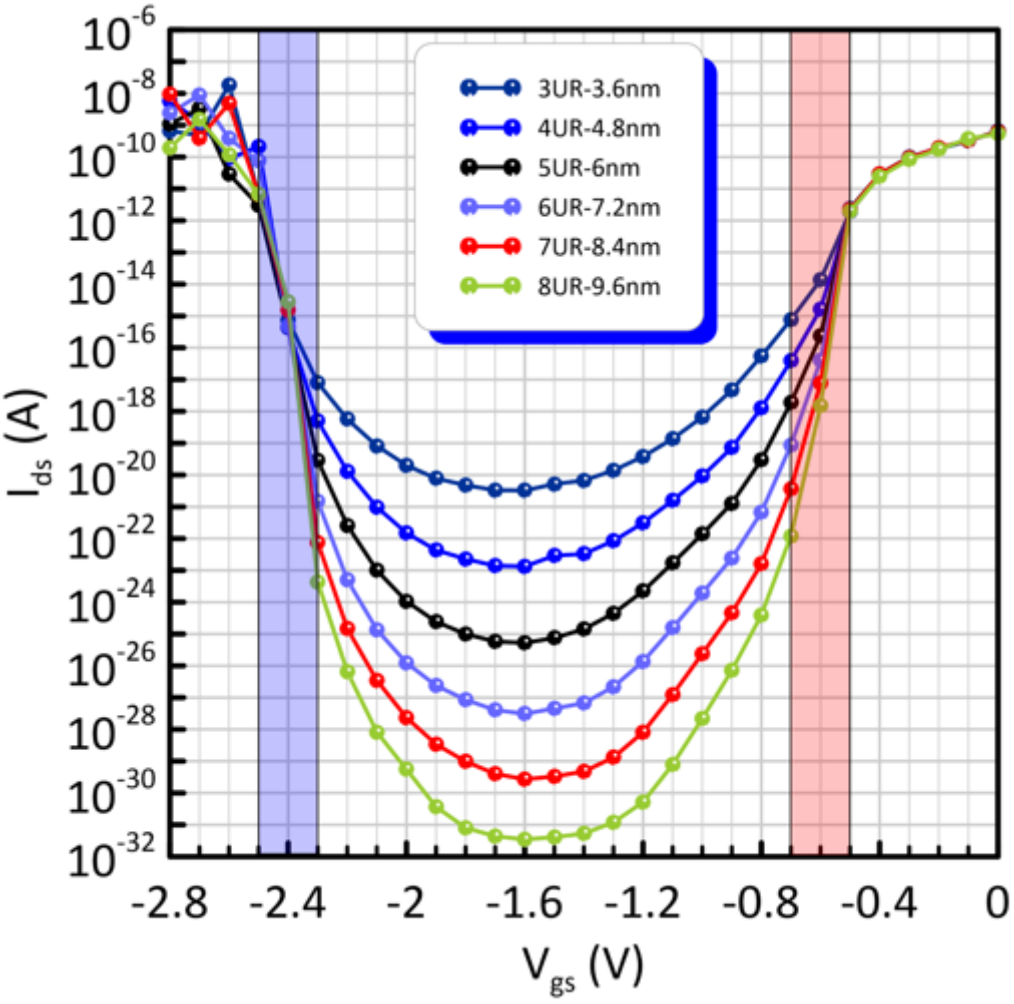

Figure 8

I-V characteristic of 3AGyNT-TFETs. Red and Blue shaded areas are operational regions of n-TFETs and p-TFETs, respectively

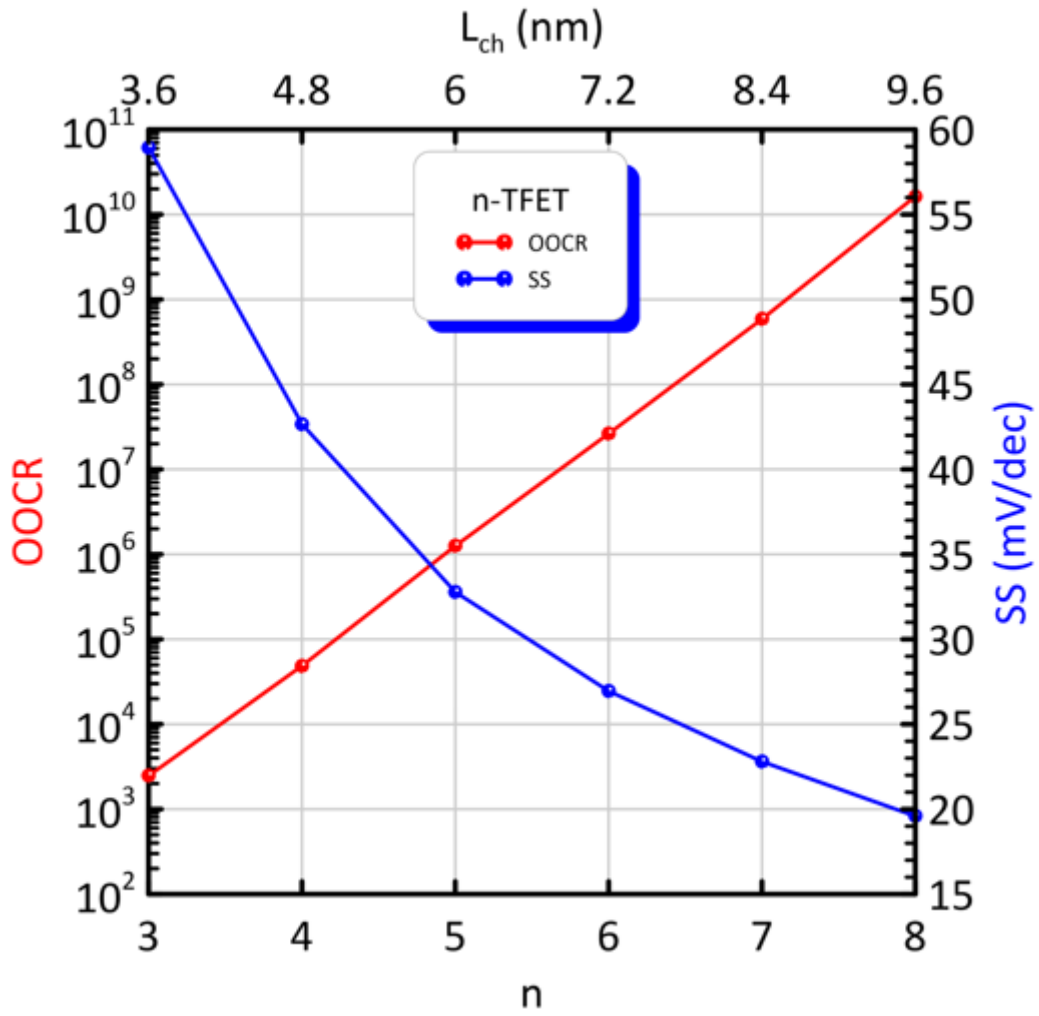

Figure 9

OOCR and SS of armchair n-TFETs versus channel length.